Electronic Supplementary Material (ESI) for New Journal of Chemistry.


*Supplementary Information*

# Ruthenium macrocycles bearing pyridine bis(carboxamide): Synthesis, structure, and catalytic activity for hydrosilylation

Hiroki Sato,[a] Tadashi Tsukamoto,[a] Hiromitsu Sogawa,[a,b] Shigeki Kuwata[a] and Toshikazu Takata*[a,c]

[a]Department of Chemical Science and Engineering, Tokyo Institute of Technology, Ookayama, Meguro-ku, Tokyo 152-8552, Japan
[b]Department of Chemistry and Materials Engineering, Faculty of Chemistry, Materials and Bioengineering, Kansai University, Suita, Osaka, 564-8680, Japan
[c]Graduate School of Advanced Science and Engineering, Hiroshima University, Kagamiyama, Higashi-Hiroshima, Hiroshima 739-8527, Japan

Corresponding author: takatats@hiroshima-u.ac.jp

Content

## 1. Supplementary Schemes, Tables and Figures

**Scheme S1**

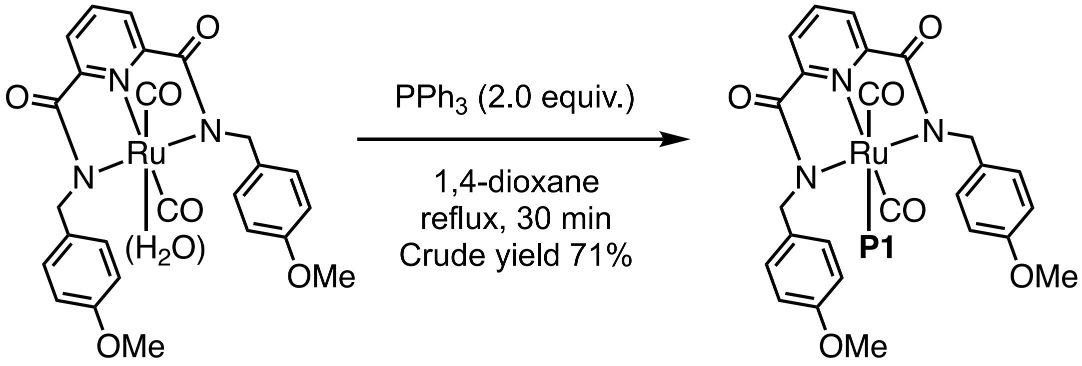


**Scheme S2**

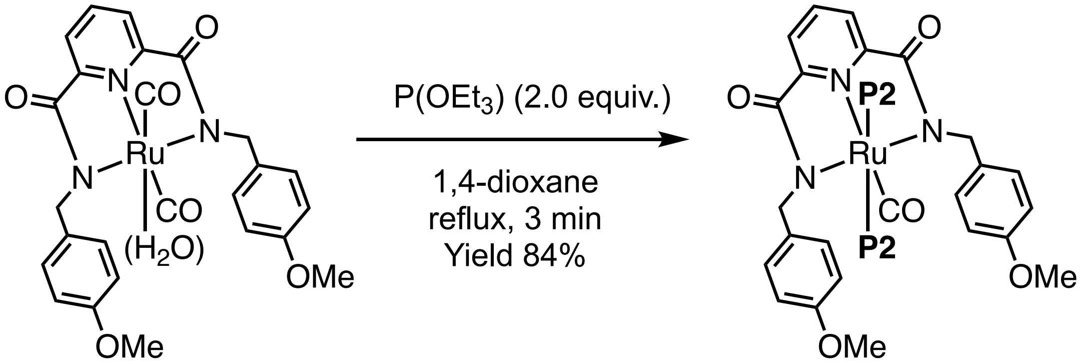

**Table S1.** Detailed conditions for the synthesis of Ru(**MC33**)$(CO)_2(H_2O)$

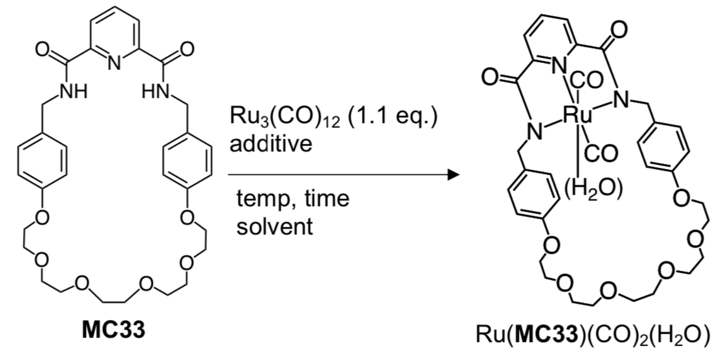


| entry | Ru south | solvent | additive | temp. / ˚C | time | result |
|---|---|---|---|---|---|---|
| 1 | $RuCl_2(PPh_3)_3$ | toluene | $NEt_3$ (10 v/v%) | 90 | 19 h | NR |
| 2 | $RuCl_2(dmso)_4$ | 2-ee | $Cs_2CO_3$ (2.0 equiv.) | 90 | 19 h | NR |
| 3 | $RuCl_2(dmso)_4$ | 2-ee | KOAc (2.2 equiv.) | 90 | 12 h | 45% conv. |
| 4 | $RuCl_2(dmso)_4$ | THF | LDA (2.4 equiv.) | 0→60 | 7 h | NR |
| 5 | $Ru_3(CO)_{12}$ | diglyme | none | 140 | 17.5 h | 13% conv. |
| 6 | $Ru_3(CO)_{12}$ | DMF | none | 140 | 8 days | 40% conv. |
| 7 | $Ru_3(CO)_{12}$ | DMF | none | 140 | 2 days | 50% conv., 10% yield |
| 8 | $Ru_3(CO)_{12}$ | DMF | 1,3,5-triaza-7-phosphaadamantane (1.1 equiv.) | 140 | 3 days | 54% conv. |
| 9 | $Ru_3(CO)_{12}$ | 2-ee | none | 140 | 2 days | 17% yield |
| 10 | $Ru_3(CO)_{12}$ | 2-ee | *p*-tolualdehyde (1.1 equiv.) | 140 | 19 h | 32% yield |
| 11 | $Ru_3(CO)_{12}$ | 2-ee | *p*-tolualdehyde (2.2 equiv.) | 140 | 15.5 h | 27% yield |
| 12 | $Ru_3(CO)_{12}$ | 2-ee | *p*-tolualdehyde (2.2 equiv.) | 120 | 19 h | 22% yield |
| 13 | $Ru_3(CO)_{12}$ | 2-ee | norbornene (1.1 equiv.) | 140 | 2 days | 35% conv. |
| 14 | $Ru_3(CO)_{12}$ | 2-ee | DIPEA (10 equiv.) | 140 | 2 days | NR |
| 15 | $Ru_3(CO)_{12}$ | 2-ee | $PPh_3$ (1.1 equiv.) | 140 | 2 days | trace |
| 16[a] | $Ru_3(CO)_{12}$ | 2-ee | CO (1 atm.) | 140 | 3 days | 42 yield |
| 17[a] | $Ru_3(CO)_{12}$ | 2-ee | CO (1 atm.) | 140 | 2 days | 97 yield |

[a]The $Ru_3(CO)_{12}$ and formed Ru(**MC33**)$(CO)_2(H_2O)$ gradually decreased by heating, leading to the decrease of the yields by prolonging the reaction time.

**Table S2.** The bond lengths and angles of Ru(**MC33**)($CO_2$)$_2$($H_2O$), Ru(**MC33**)($CO_2$)$_2$(**P1**), and Ru(**AC**)($CO_2$)$_2$($H_2O$)

| compound | IR ($cm^{-1}$) | | X-ray | | | | | |
|---|---|---|---|---|---|---|---|---|
| | s | as | Ru1-N1 (Å) | Ru1-N2 (Å) | Ru1-N3 (Å) | C-O (Ax.) (Å) | C-O (Eq.) (Å) | ∠N2Ru1N3 (°) |
| Ru(**MC33**)($CO_2$)$_2$($H_2O$) | 2046 | 1977 | 2.031(3) | 2.101(3) | 2.104(4) | 1.138(3) | 1.151(5) | 155.1(1) |
| Ru(**MC33**)($CO_2$)$_2$(**P1**) | 2060 | 1977 | 2.026(4) | 2.126(4) | 2.087(3) | 1.120(6) | 1.165(2) | 154.5(1) |
| Ru(**AC**)($CO_2$)$_2$($H_2O$) | 2046 | 1977 | 2.024(2) | 2.112(2) | 2.100(2) | 1.146(3) | 1.144(3) | 155.3 8) |

**Table S3.** The bond lengths and angles of Ru(**MC33**)(CO)(**P2**)$_2$

| compound | IR ($cm^{-1}$) | | X-ray | | | | |
|---|---|---|---|---|---|---|---|
| | s | as | Ru1-N1 / Ru2-N4 (Å) | Ru1-N2 / Ru2-N5 (Å) | Ru1-N3 / Ru2-N6 (Å) | C44-O15 / C88-O30 (Eq.) (Å) | ∠N2Ru1N3 / ∠N5Ru2N6 (°) |
| Ru(**MC33**)(CO)(**P2**)$_2$ | 1959 | – | 2.042(3) / 2.048(4) | 2.115(4) / 2.110(3) | 2.102(3) / 2.125(3) | 1.163(5) / 1.148(6) | 154.4(1) / 153.5(1) |

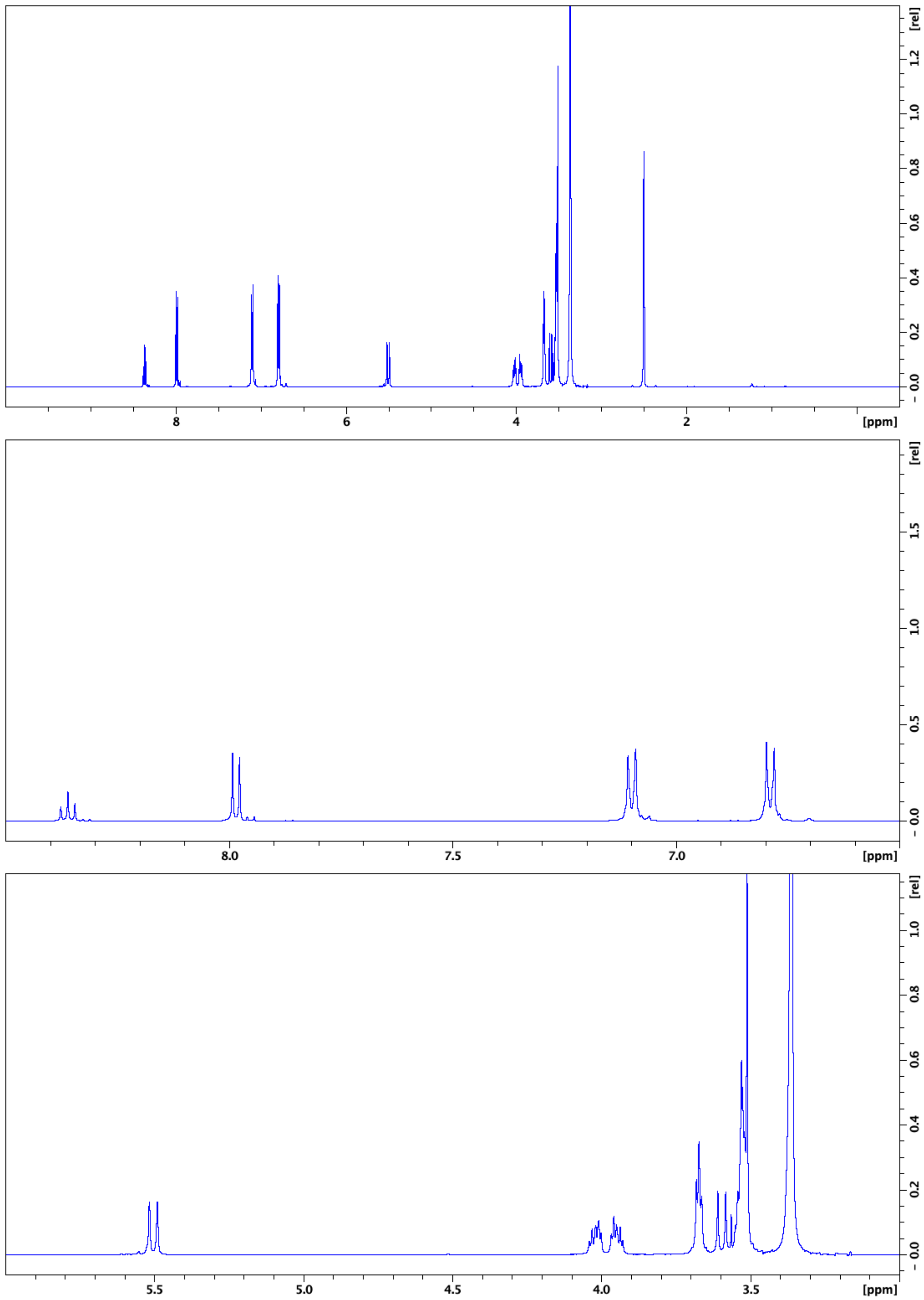


**Fig. S1.** $^{1}$H-NMR spectra of Ru(**MC33**)$(CO)_2(H_2O)$ (500 MHz, DMSO-$d_6$, r.t.).

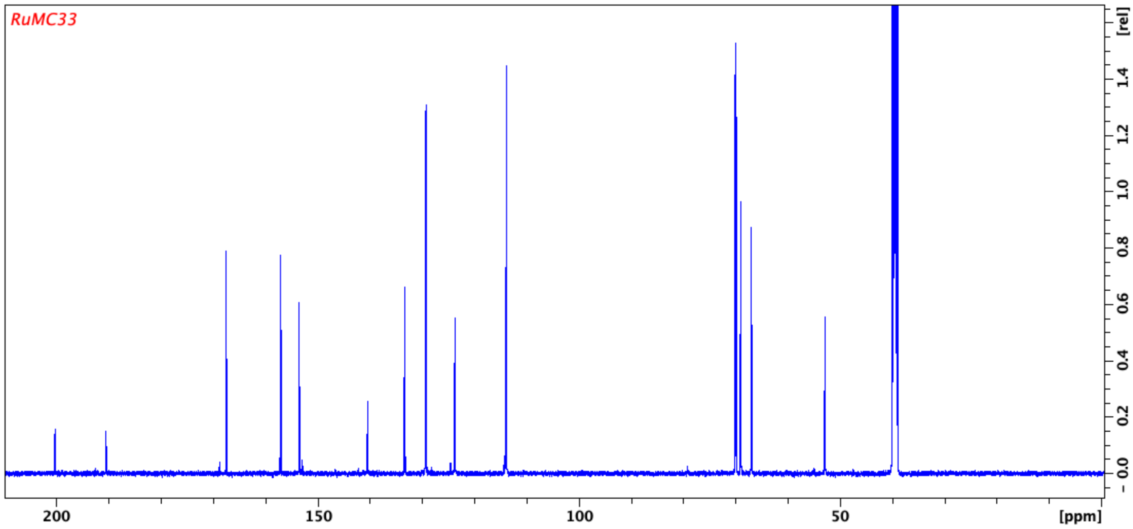


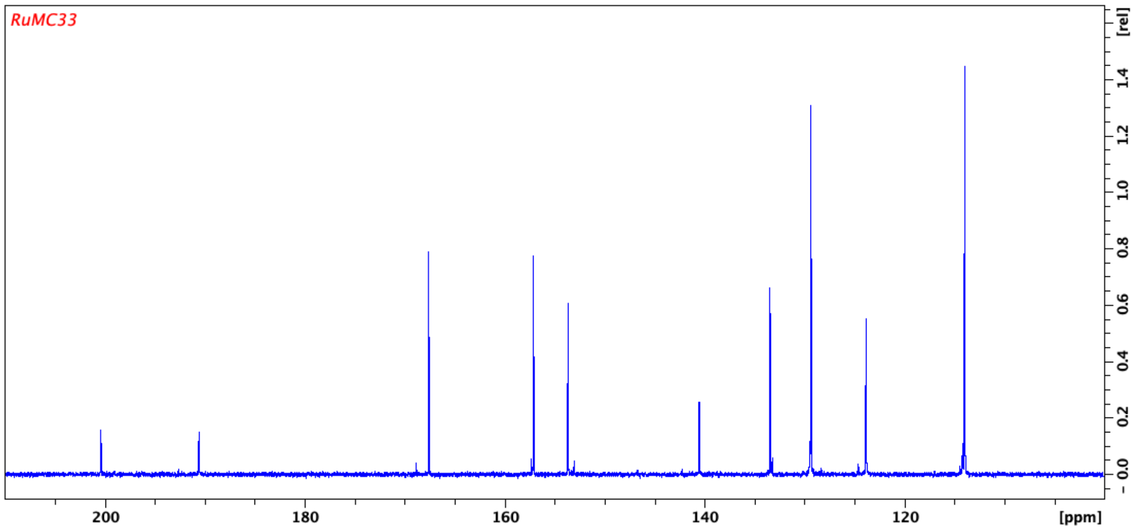


**Fig. S2.** $^{13}$C-NMR spectra of Ru(**MC33**)$(CO)_2(H_2O)$ (125 MHz, DMSO-$d_6$, r.t.).

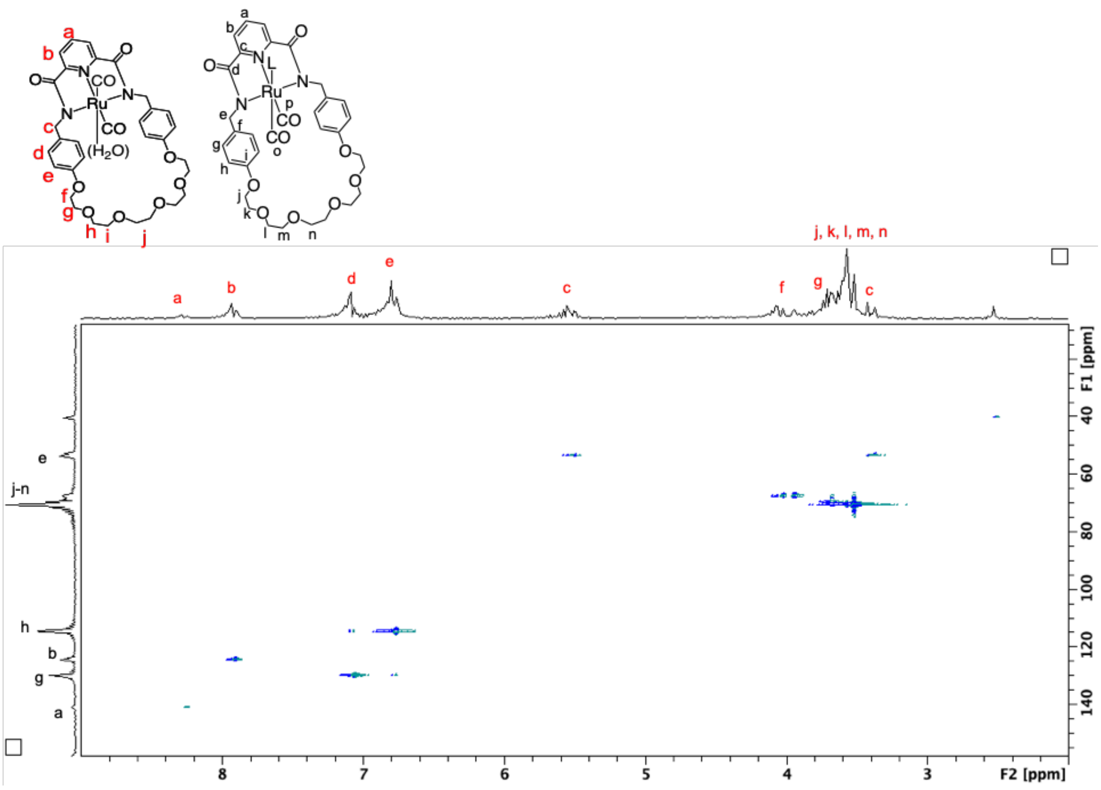

**Fig. S3.** HSQC spectrum of Ru(**MC33**)$(CO)_2(H_2O)$ (DMSO-$d_6$).

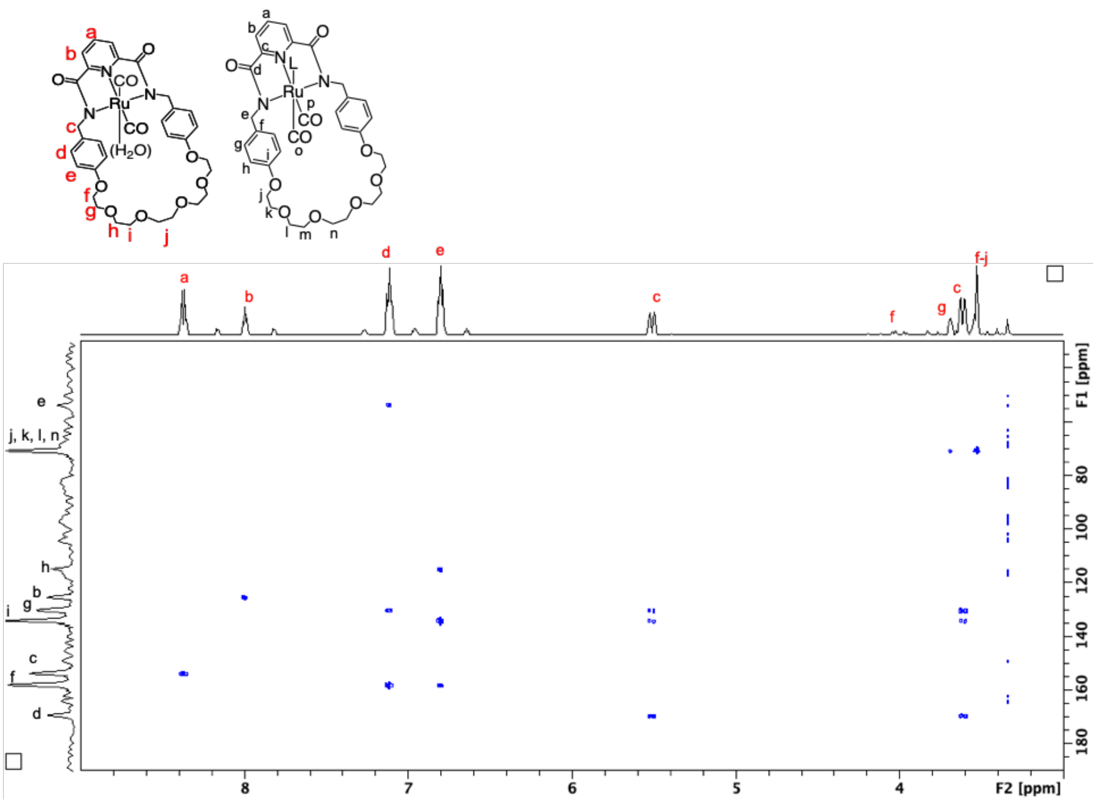

**Fig. S4.** HMBC spectrum of Ru(**MC33**)$(CO)_2(H_2O)$ (DMSO-$d_6$).

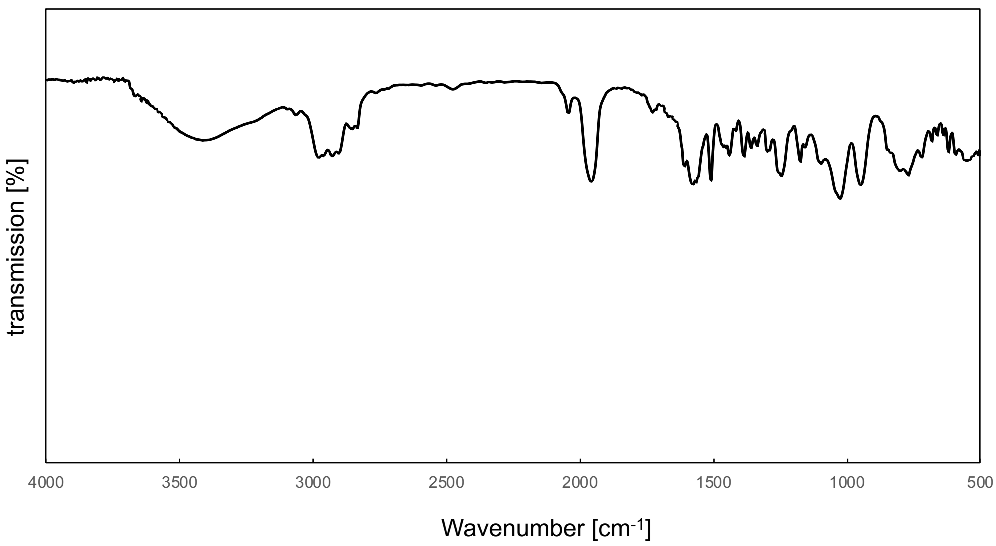


**Fig. S5.** FT-IR spectrum of Ru(**MC33**)$(CO)_2(H_2O)$.

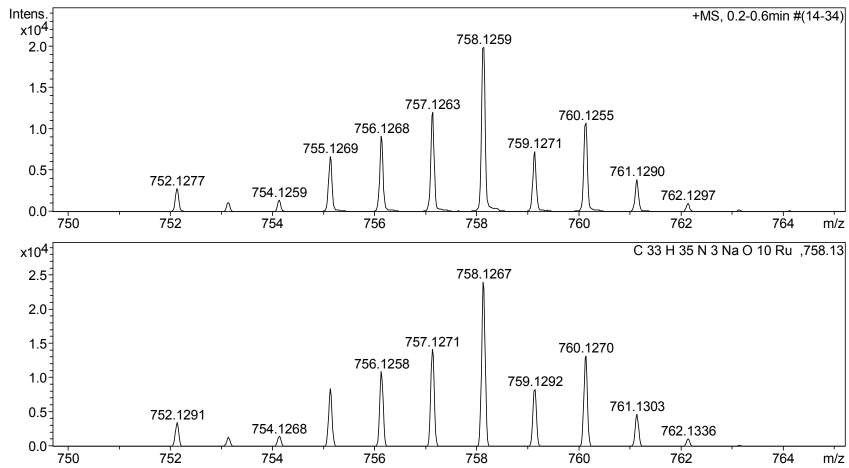


**Fig. S6.** ESI-TOF-MS spectrum of [Ru(**MC33**)$(CO)_2$+Na]$^+$ (positive) (upper: found, bottom: calculated for $C_{33}H_{35}N_3NaO_{10}Ru$). Note that $H_2O$ was dissociated from complex during MS measurement.

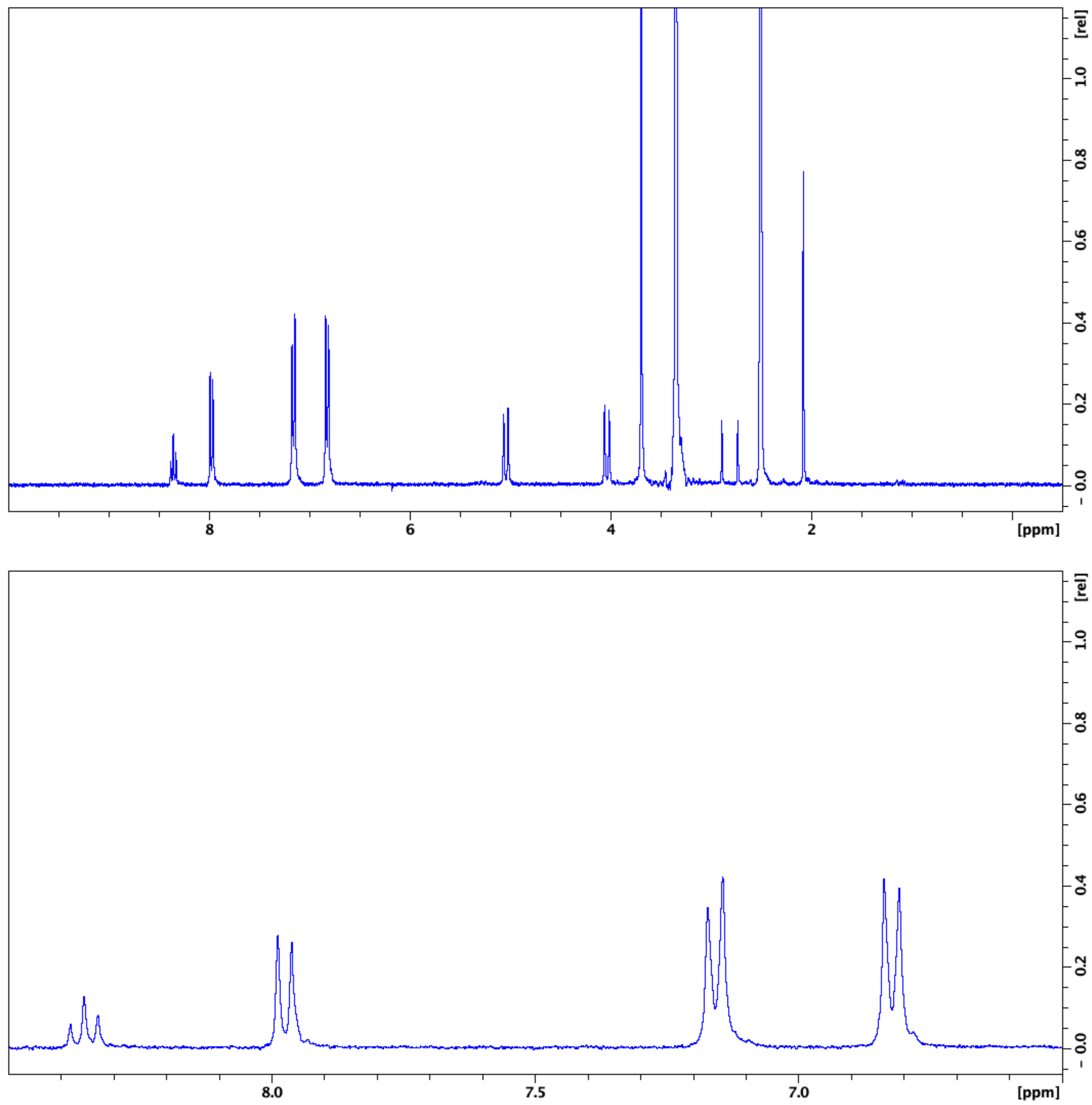


**Fig. S7.** $^{1}$H-NMR spectra of Ru(**AC**)$(CO)_2(H_2O)$ (500 MHz, DMSO-$d_6$, r.t.).

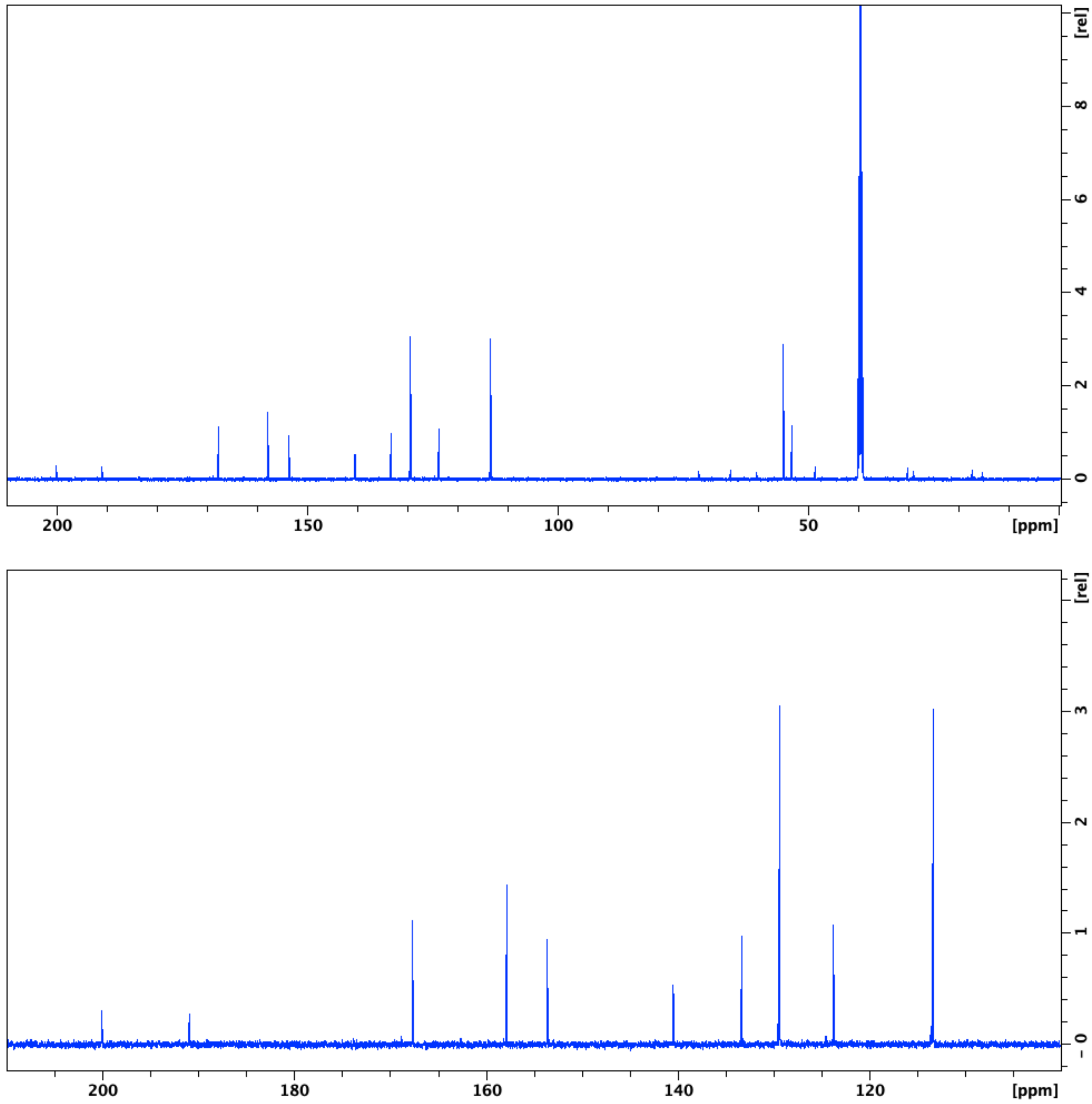


**Fig. S8.** $^{13}$C-NMR spectra of Ru(**AC**)$(CO)_2(H_2O)$ (125 MHz, DMSO-$d_6$, r.t.).

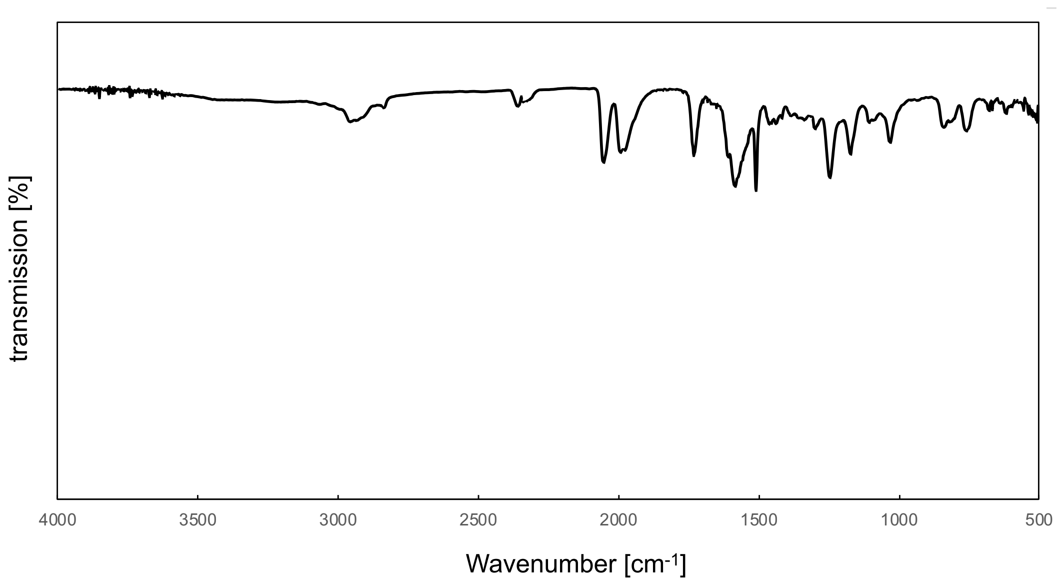


**Fig. S9.** FT-IR spectrum of Ru(**AC**)$(CO)_2(H_2O)$.

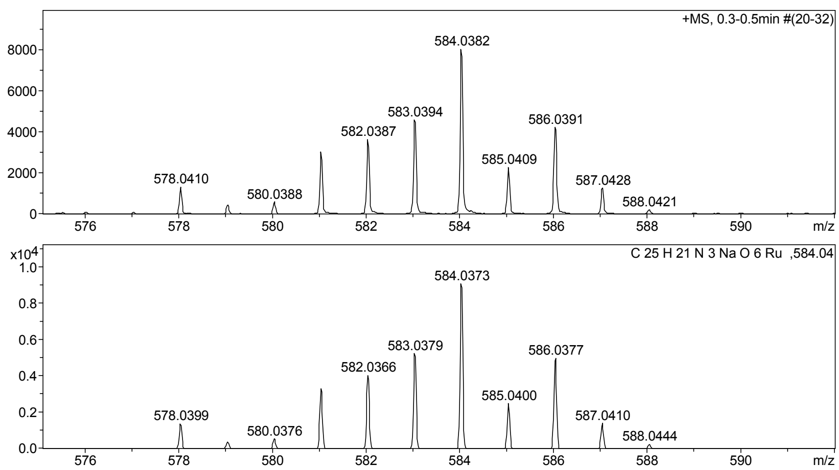


**Fig. S10.** ESI-TOF-MS spectrum of [Ru(**AC**)$(CO)_2$+Na]$^+$ (positive) (upper: found, bottom: calculated for $C_{25}H_{21}N_3NaO_6Ru$). Note that $H_2O$ was dissociated from complex during MS measurement.

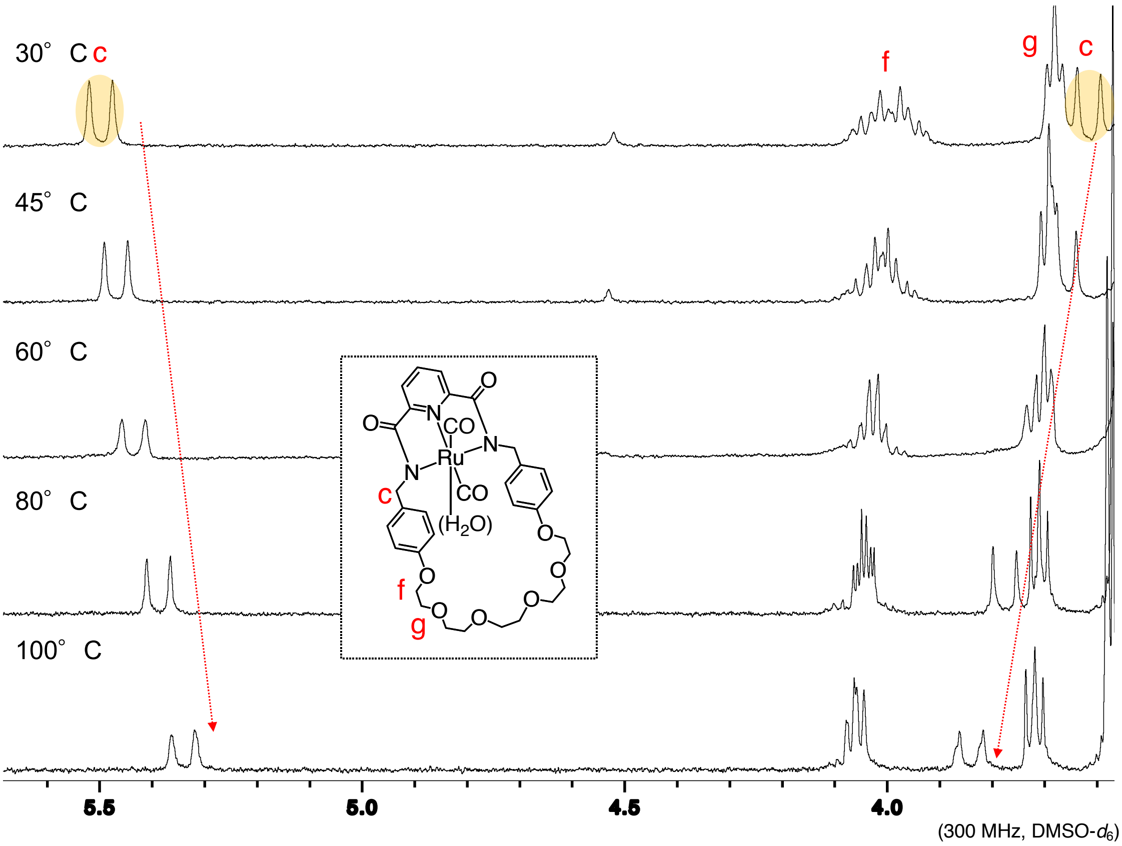


**Fig. S11.** VT-NMR spectra of Ru(**MC33**)$(CO)_2(H_2O)$ (300 MHz, DMSO-$d_6$).

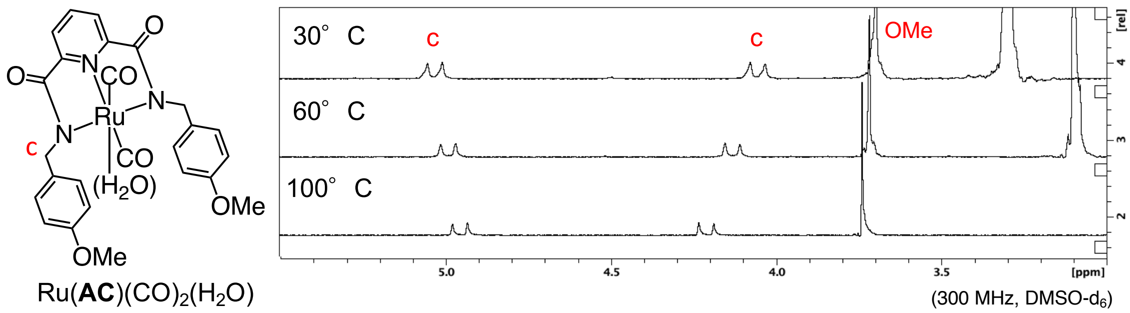


**Fig. S12.** VT-NMR spectra of Ru(**AC**)$(CO)_2(H_2O)$ (300 MHz, DMSO-$d_6$).

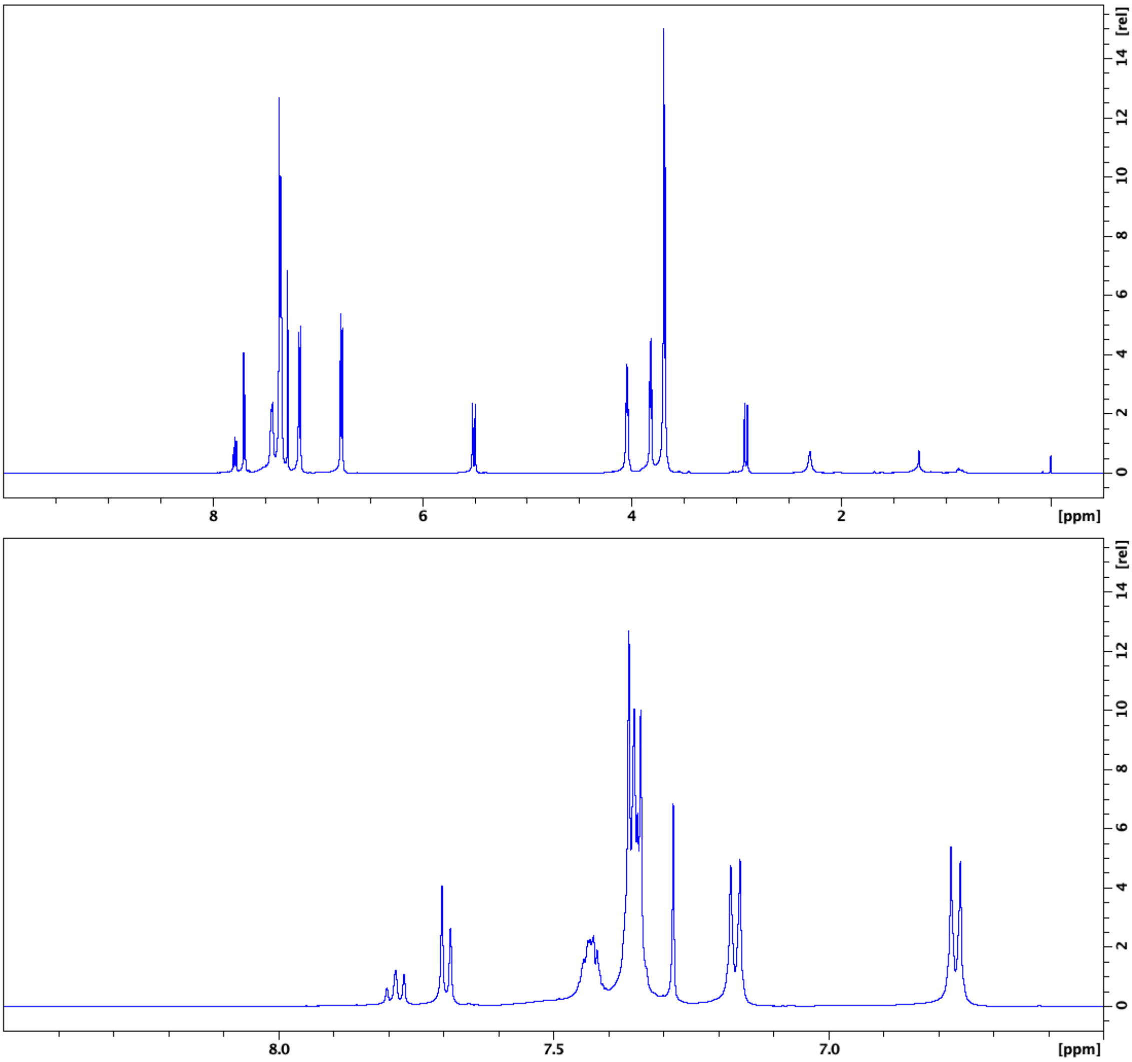


**Fig. S13.** $^{1}$H-NMR spectra of Ru(**MC33**)$(CO)_2$(**P1**) (500 MHz, $CDCl_3$, r.t.).

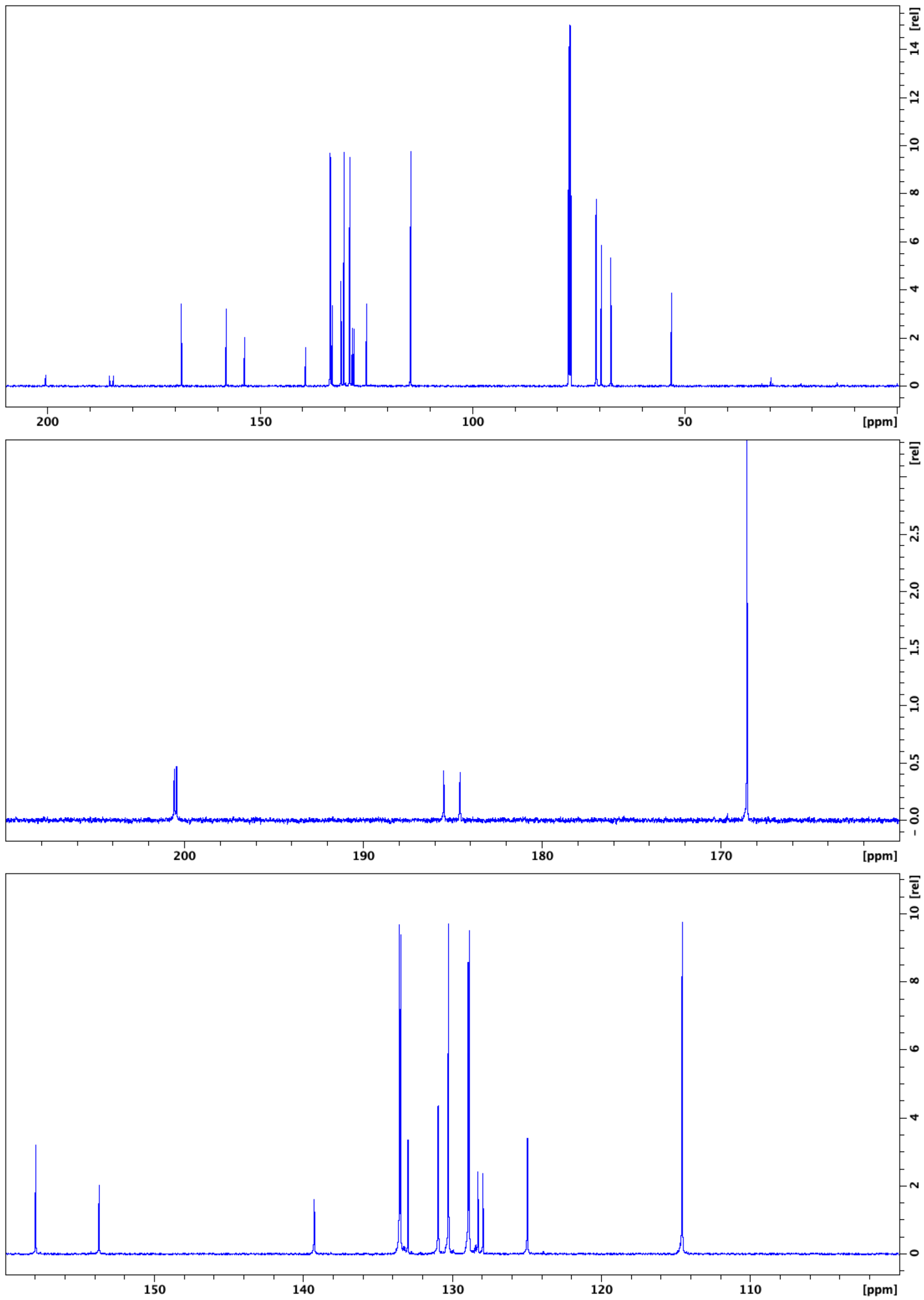


**Fig. S14.** $^{13}$C-NMR spectra of Ru(**Ru33**)$(CO)_2$(**P1**) (125 MHz, $CDCl_3$, r.t.).

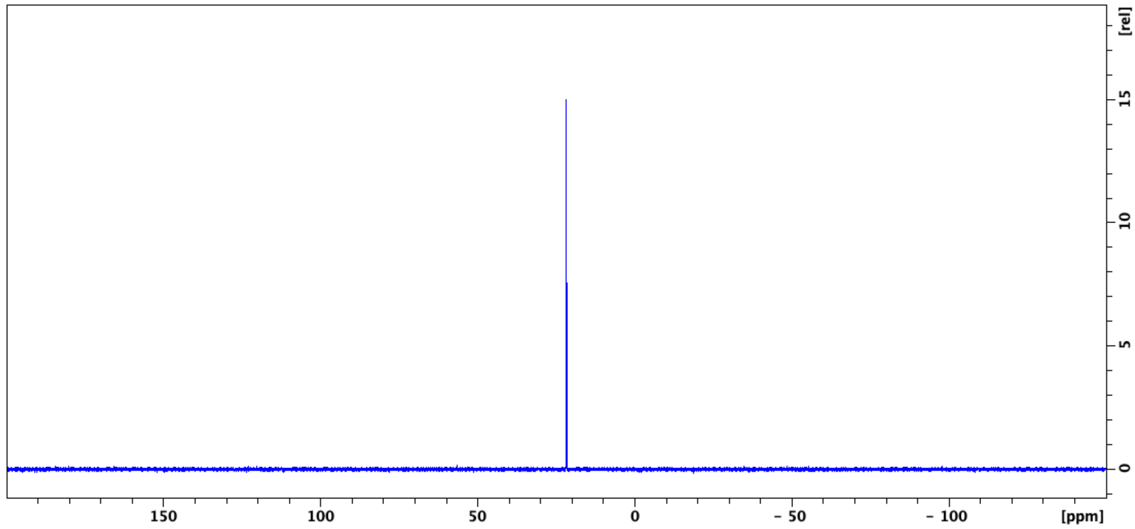


**Fig. S15.** $^{31}$P-NMR spectrum of Ru(**MC33**)$(CO)_2$(**P1**) (202 MHz, DMSO-$d_6$, r.t.).

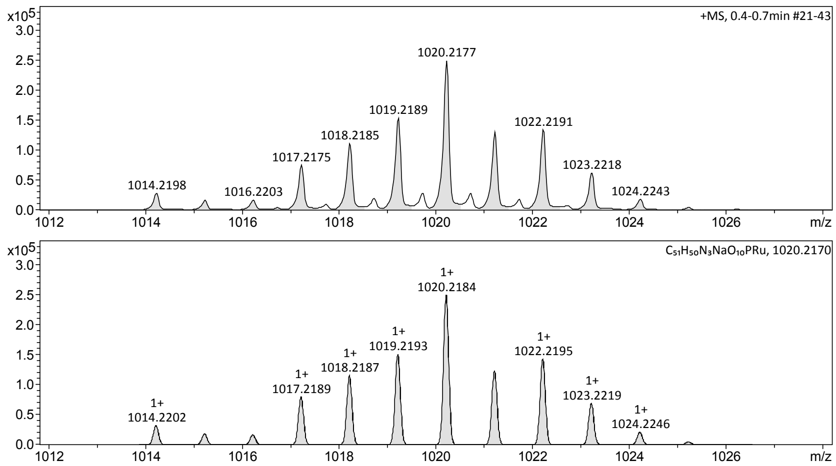


**Fig. S16.** ESI-TOF-MS spectrum of [Ru(**MC33**)$(CO)_2$(**P1**)+Na]$^+$positive) (upper: found, bottom: calculated for $C_{51}H_{50}N_3NaO_{10}PRu$).

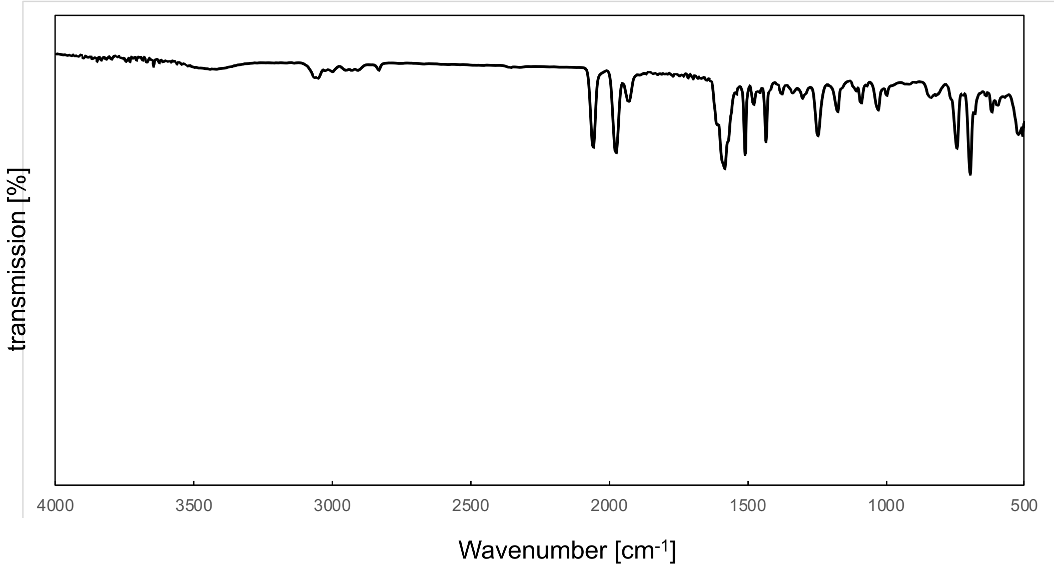


**Fig. S17.** FT-IR spectrum of Ru(**MC33**)(CO)$_2$(**P1**).

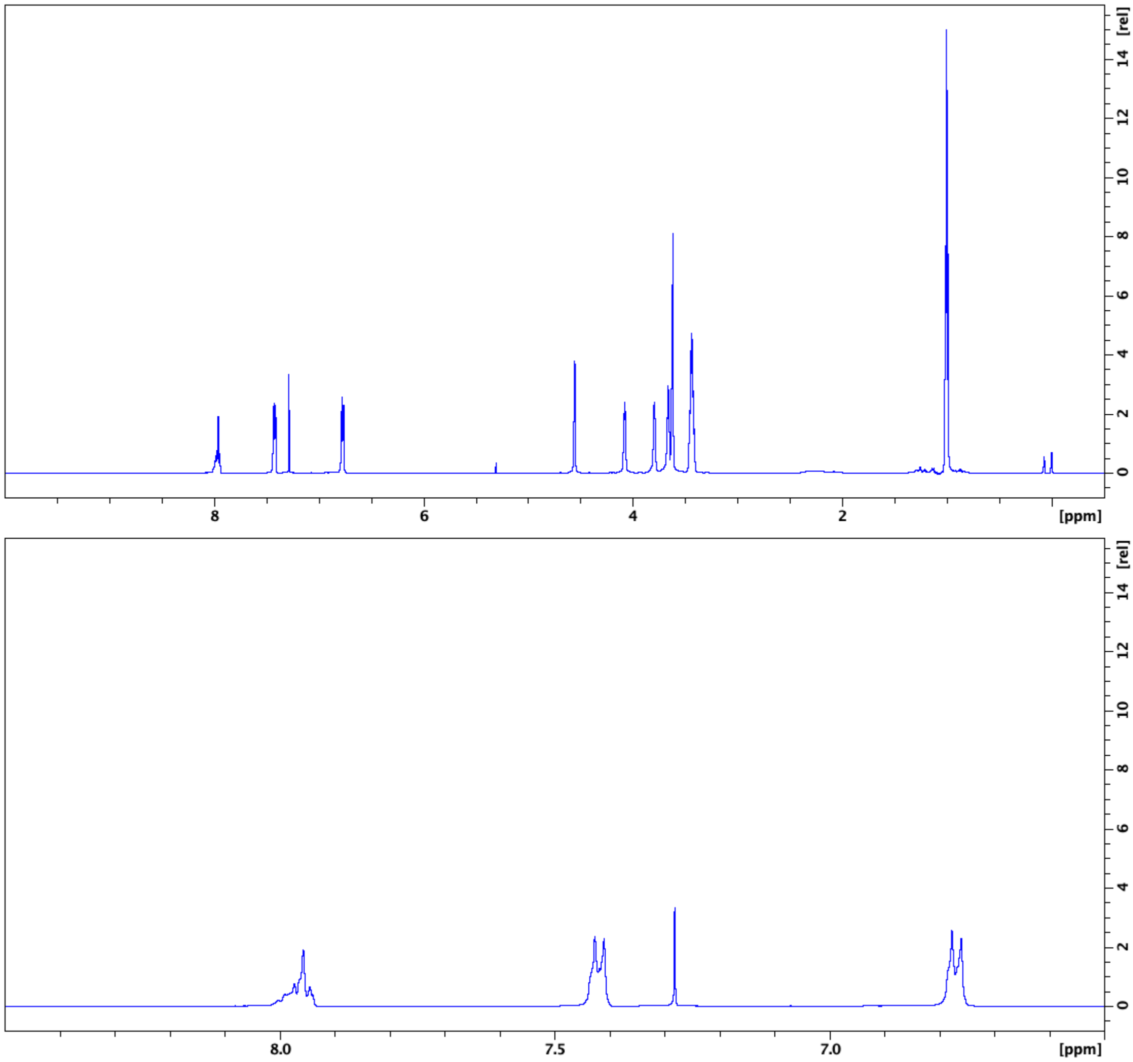

**Fig. S18.** $^1$H-NMR spectra of Ru(**MC33**)(CO)(**P2**)$_2$ (500 MHz, $CDCl_3$, r.t.).

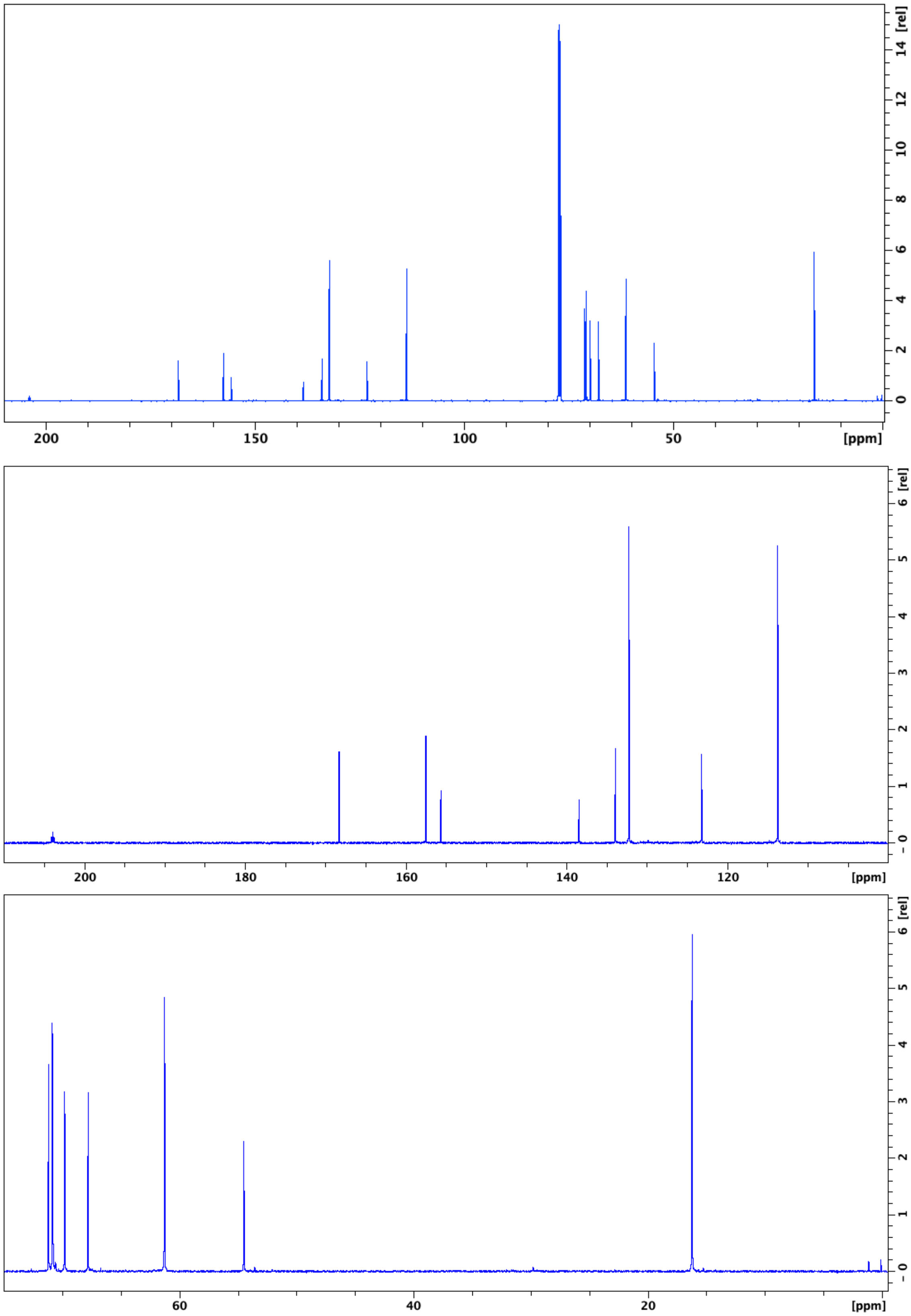


**Fig. S19.** $^{13}$C-NMR spectra of Ru(**MC33**)(CO)(**P2**)$_2$ (125 MHz, $CDCl_3$, r.t.).

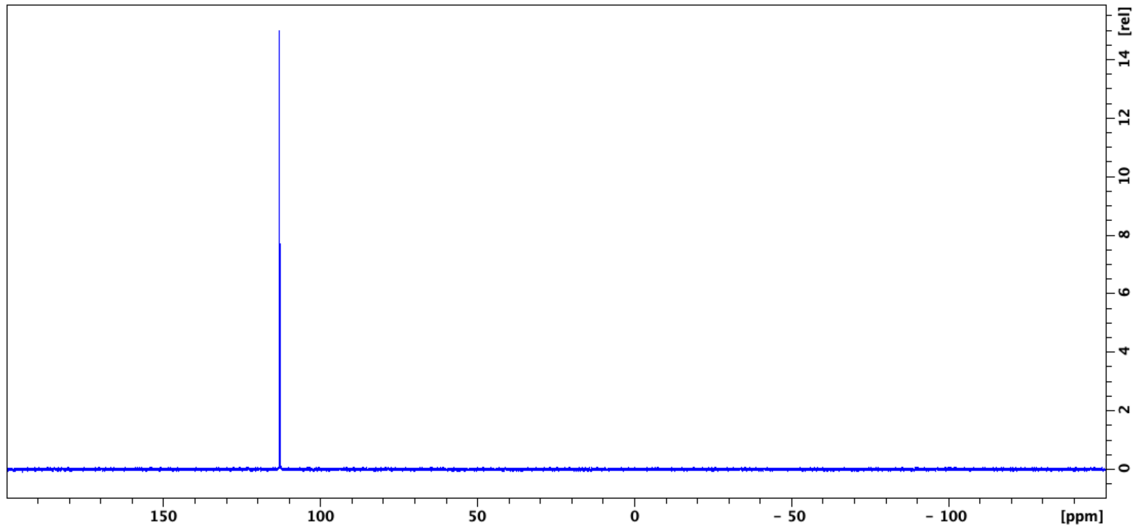


**Fig. S20.** $^{31}P$-NMR spectrum of Ru(**MC33**)(CO)(**P2**)$_2$ (202 MHz, $CDCl_3$, r.t.).

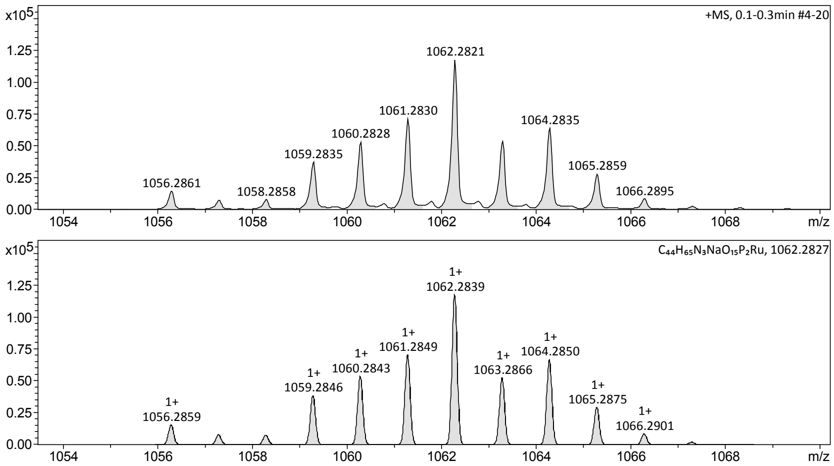


**Fig. S21.** ESI-TOF-MS spectrum of [Ru(**MC33**)(CO)(**P2**)$_2$+Na]$^+$ (positive) of (upper: found, bottom: calculated for $C_{44}H_{65}N_3NaO_{15}P_2Ru$)

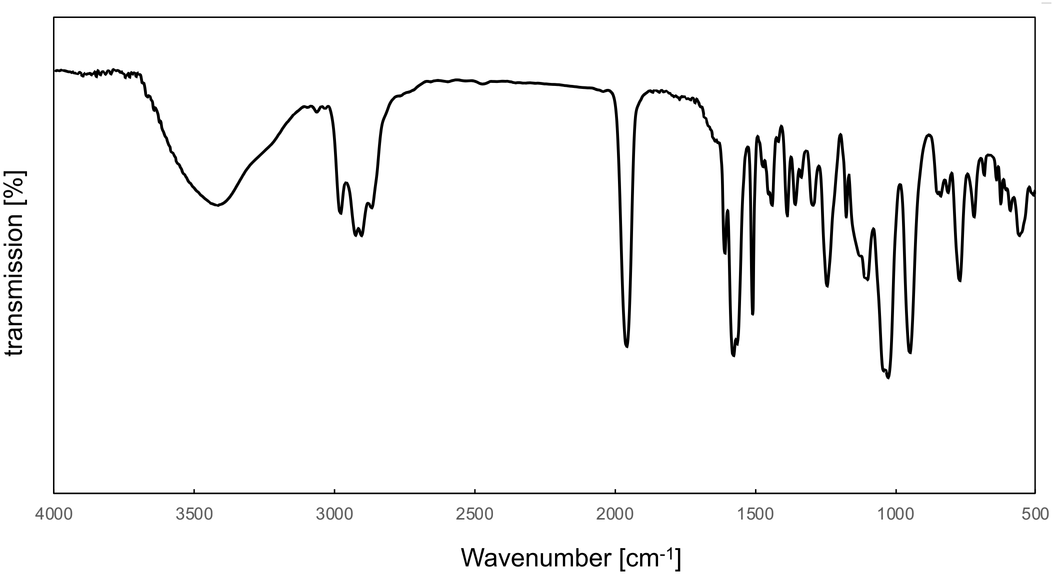


**Fig. S22.** FT-IR spectrum of Ru(**MC33**)(CO)(**P2**)$_2$.

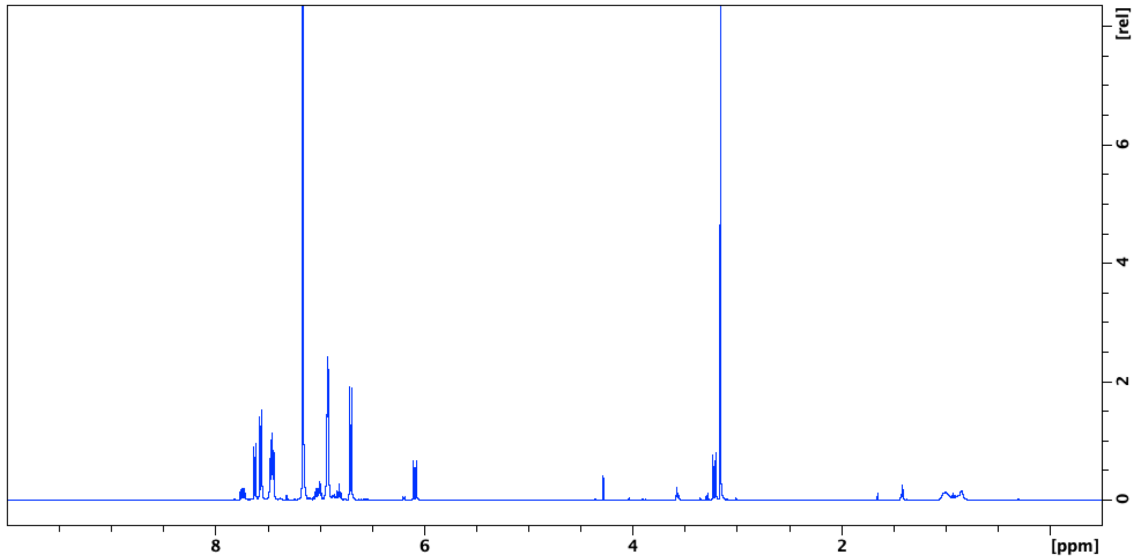


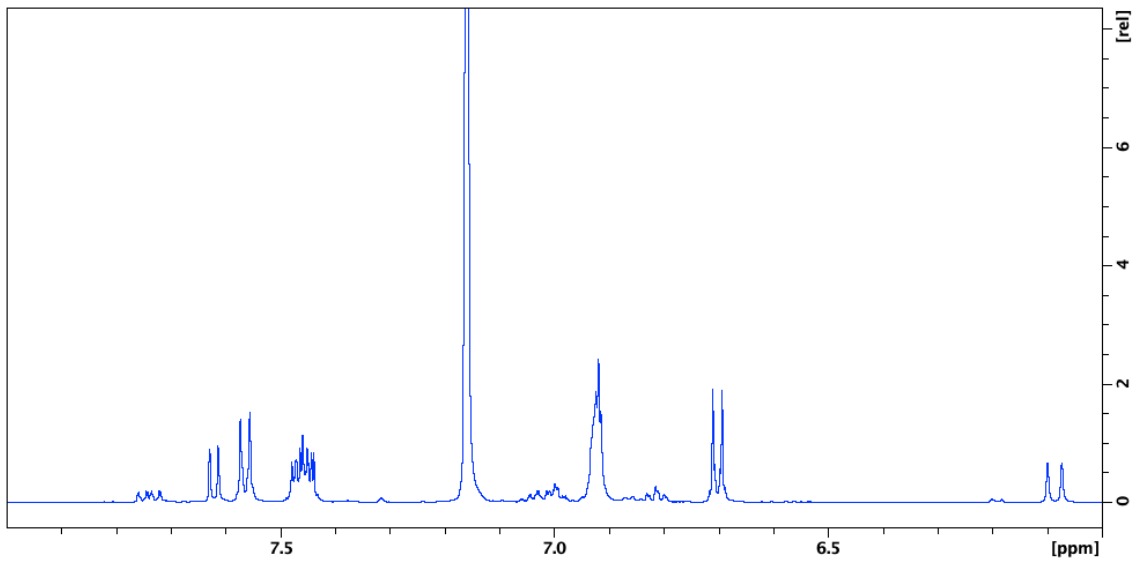


**Fig. S23.** $^{1}$H-NMR spectra of Ru(**AC**)$(CO)_2$(**P1**) (not isolated, crude product) (500 MHz, $C_6D_6$, r.t.).

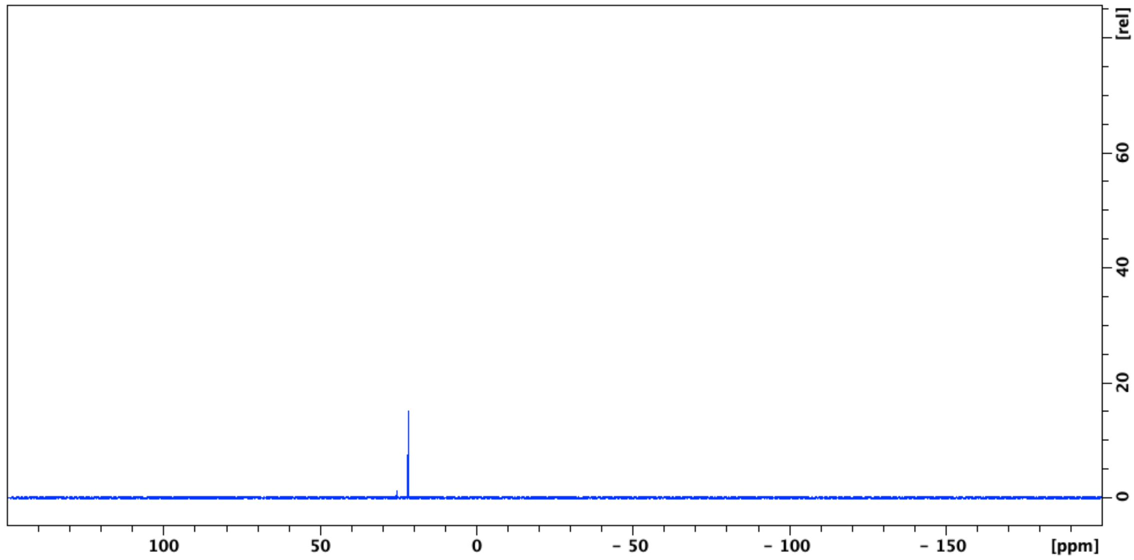


**Fig. S24.** $^{31}$P-NMR spectrum of Ru(**AC**)(CO)$_2$(**P1**) (not isolated, crude product) (202 MHz, $C_6D_6$, r.t.).

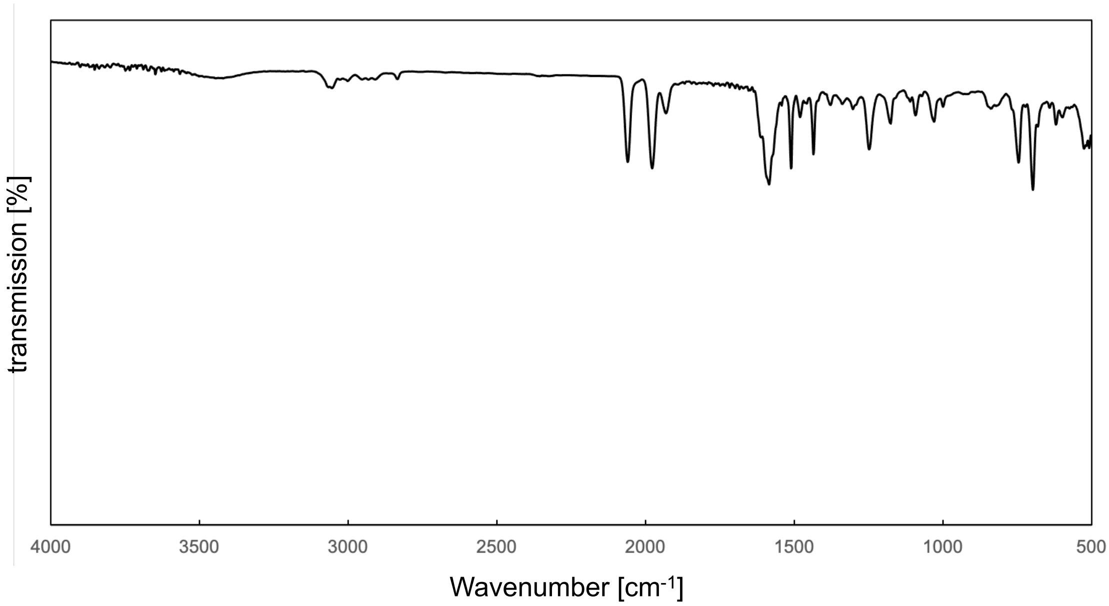


**Fig. S25.** FT-IR spectrum of Ru(**AC**)(CO)$_2$(**P1**) (not isolated, crude product).

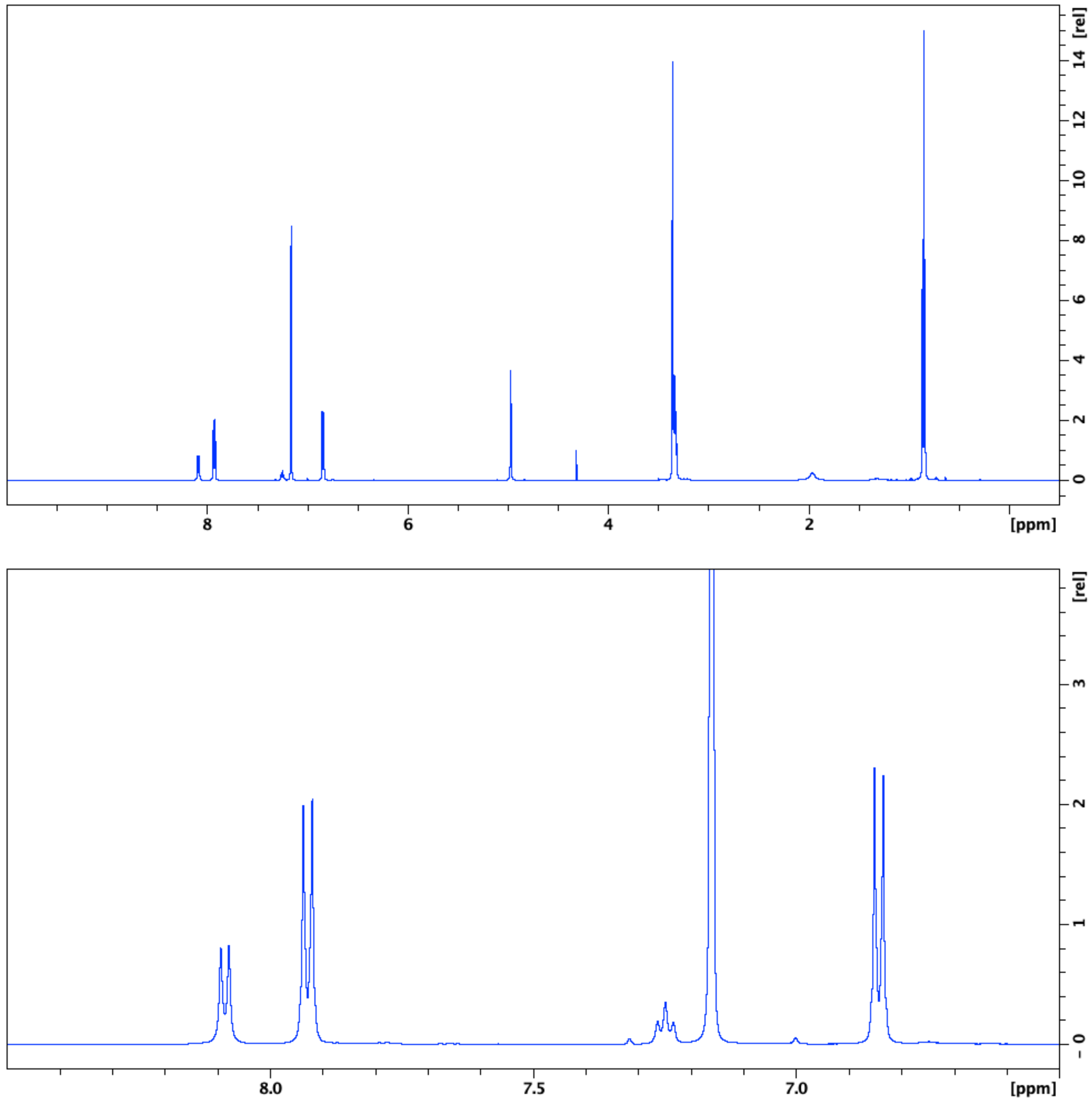


**Fig. S26.** $^{1}$H-NMR spectra of Ru(**AC**)(CO)(**P2**)$_2$ (500 MHz, $C_6D_6$, r.t.).

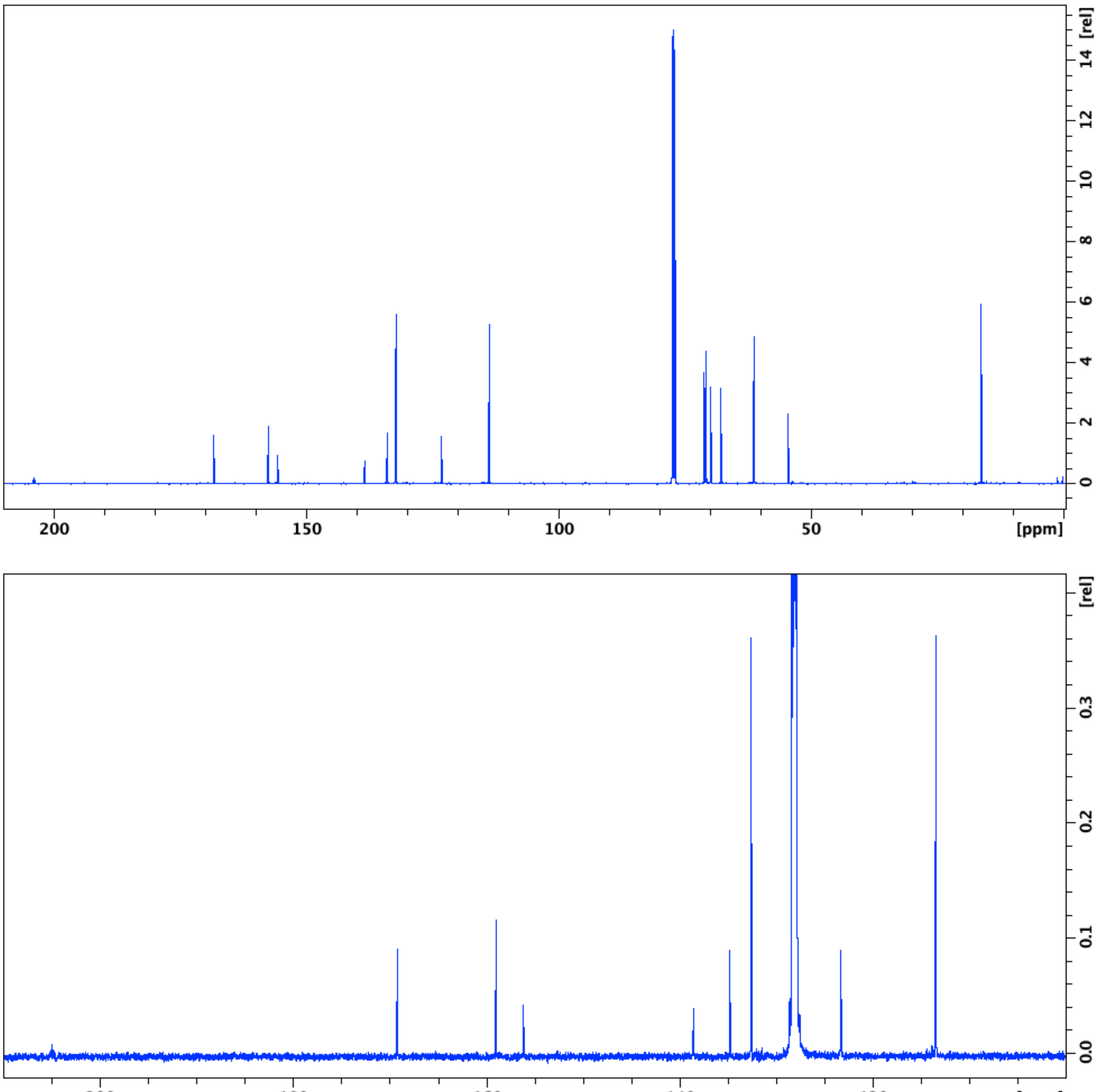


**Fig. S27.** $^{13}$C-NMR spectra of Ru(**AC**)(CO)(**P2**)$_2$ (125 MHz, $C_6D_6$, r.t.).

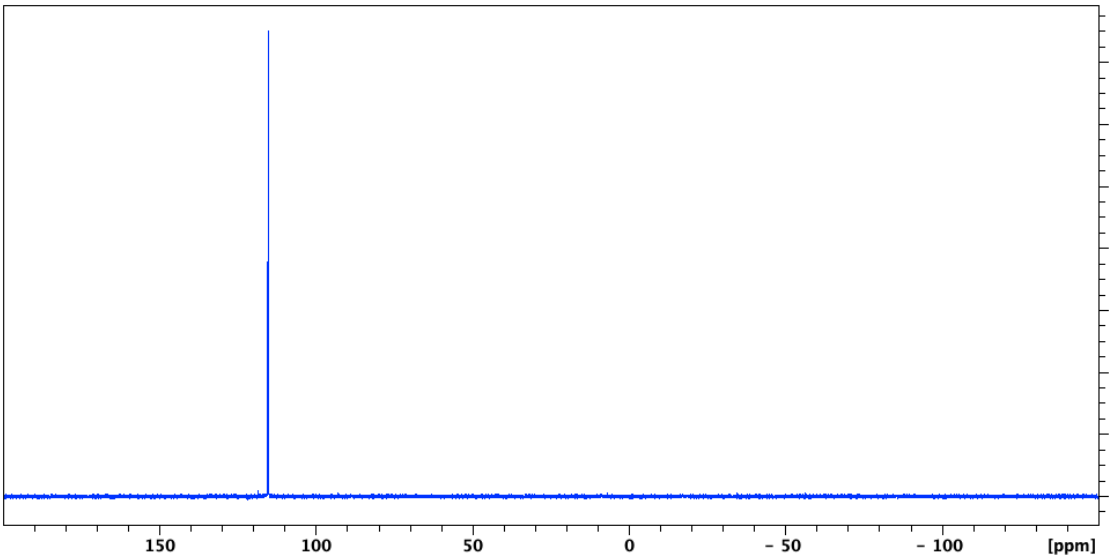


**Fig. S28.** $^{31}$P-NMR spectrum of Ru(**AC**)(CO)(**P2**)$_2$ (202 MHz, $C_6D_6$, r.t.).

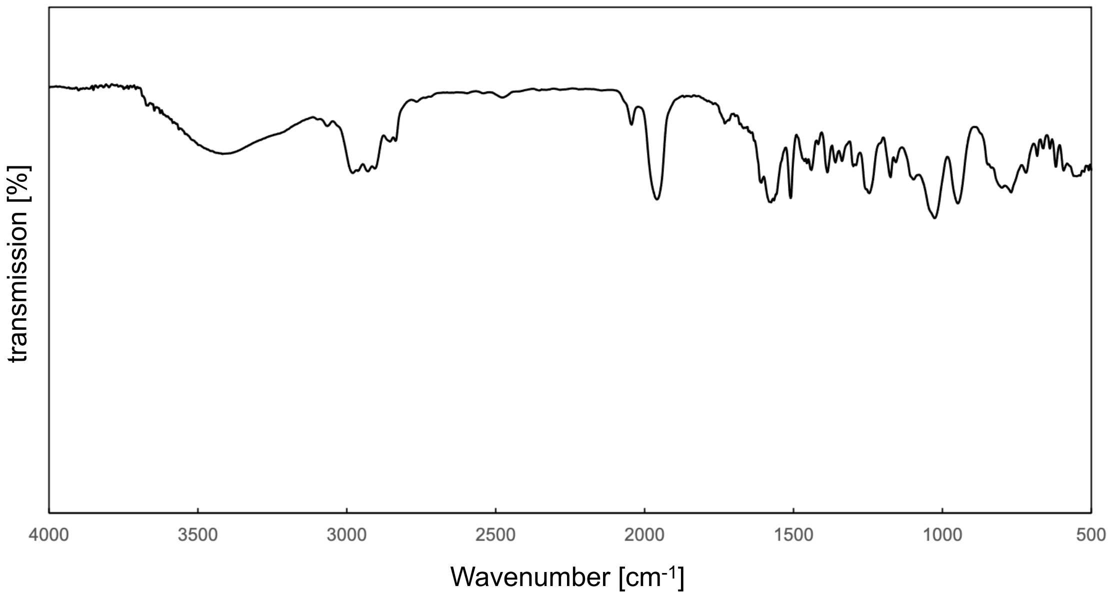


**Fig. S29.** FT-IR spectrum of Ru(**AC**)(CO)(**P2**)$_2$.

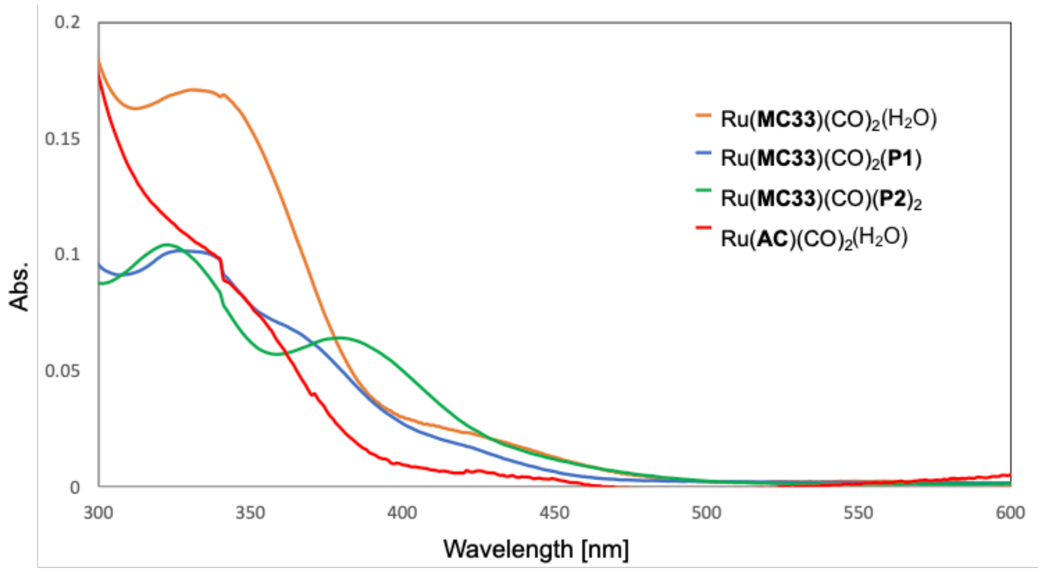


**Fig. S30.** UV-vis spectra of Ru complexes in DMSO.

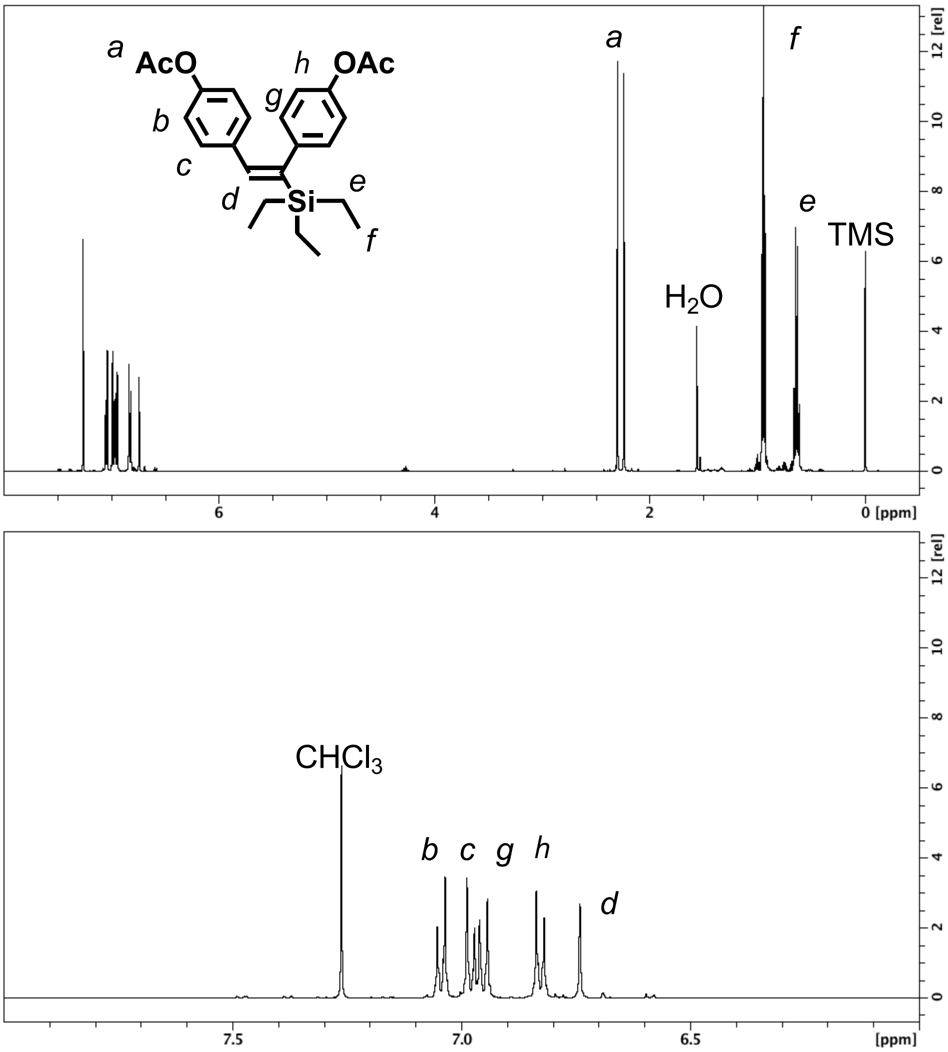


**Fig. S31.** [1]H-NMR spectrum of *cis*-vinylsilane **2** (500 MHz, $CDCl_3$, r.t.).

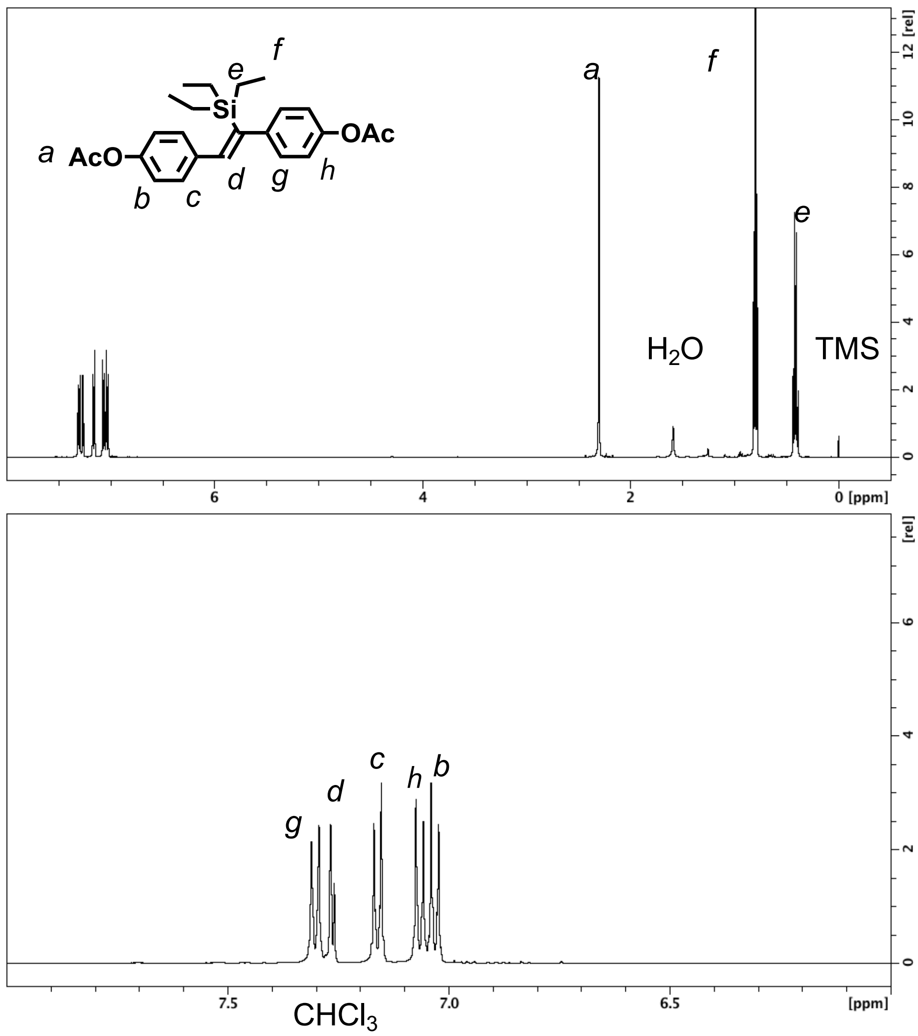


**Fig. S32.** $^1$H-NMR spectrum of *trans*-vinylsilane **3** (500 MHz, $CDCl_3$, r.t.).

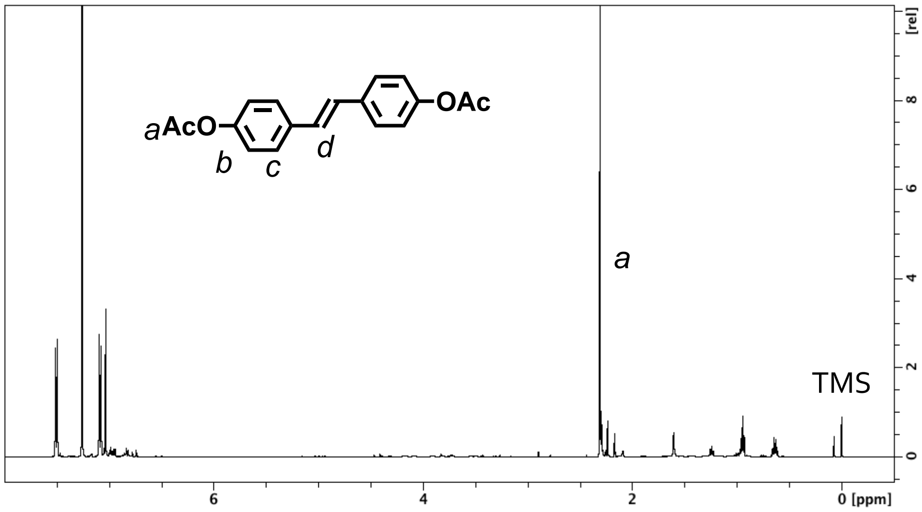


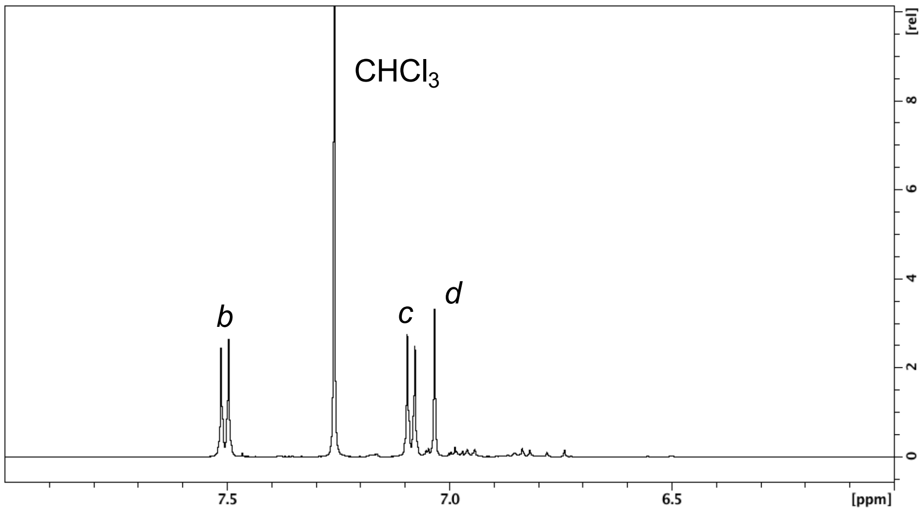


**Fig. S33.** $^1$H-NMR spectrum of *trans*-stylbene **4** (500 MHz, $CDCl_3$, r.t.).

## 2. X-ray Crystallographic Data

A single crystal of Ru(**MC33**)$(CO)_2(H_2O)$ was obtained by the recrystallization from water vapor diffusion into a DMF solution of the compound.

Crystal data of Ru(**MC33**)$(CO)_2(H_2O)$: $C_{34.3}H_{41.56}N_{3.65}O_{11}Ru$, red prism, 0.19 × 0.05 × 0.05 $mm^3$, triclinic, space group *P*-1 (#2), $a$ = 10.629(4) Å, $b$ = 12.451(4) Å, $c$ = 15.252(5) Å, $\alpha$ = 68.755(18)°, $\beta$ = 77.07(2)°, $\gamma$ = 74.08(2)°, $V$ = 1791.5(11) Å$^3$, $\rho_{calcd}$ = 1.450 g/cm$^3$, $Z$ = 2, 14821 reflections measured, $R1$ = 0.0490 [$I > 2\sigma(I)$], and $wR2$ = 0.1229 (all reflections), GOF = 0.986.

A single crystal of Ru(**MC33**)$(CO)_2$(**P1**) was obtained by recrystallization from a benzene solution.

Crystal data of Ru(**MC33**)$(CO)_2$(**P1**): $C_{51}H_{52}N_3O_{11}PRu$, orange prism, 0.24 × 0.13 × 0.12 $mm^3$, triclinic, space group *P*-1 (#2), $a$ = 12.906(8) Å, $b$ = 13.325(8) Å, $c$ = 14.696(8) Å, $\alpha$ = 78.66(3)°, $\beta$ = 73.19(3)°, $\gamma$ = 84.04(3)°, $V$ = 2369(2) Å$^3$, $\rho_{calcd}$ = 1.423 g/cm$^3$, $Z$ = 2, 19292 reflections measured, $R1$ = 0.0573 [$I > 2\sigma(I)$], and $wR2$ = 0.1454 (all reflections), GOF = 0.896.

A single crystal of Ru(**MC33**)(CO)(**P2**)$_2$ was obtained by liquid-liquid diffusion crystallization ($CH_2Cl_2$/hexane = 1/9).

Crystal data of Ru(**MC33**)(CO)[ **P2**]$_2$·$2CH_2Cl_2$·$H_2O$: $C_{46}H_{71}Cl_4N_3O_{16}P_2Ru$, yellow prism, 0.24 × 0.23 × 0.06 $mm^3$, triclinic, space group *P*-1 (#2), $a$ = 12.256(3) Å, $b$ = 20.547(4) Å, $c$ = 23.363(5) Å, $\alpha$ = 99.334(3)°, $\beta$ = 99.324(4)°, $\gamma$ = 98.5572(16)°, $V$ = 5635(2) Å$^3$, $\rho_{calcd}$ = 1.446 g/cm$^3$, $Z$ = 4, 70352 reflections measured, $R1$ = 0.0761 [$I > 2\sigma(I)$], and $wR2$ = 0.2095 (all reflections), GOF = 1.065.

A single crystal of Ru(**AC**)$(CO)_2$(dmf) was obtained by recrystallization from a DMF/water solution.

Crystal data of Ru(**AC**)$(CO)_2$(dmf)·DMF: $C_{28}H_{30}N_4O_8Ru$, yellow prism, 0.15 × 0.15 × 0.11 $mm^3$, monoclinic, space group $P2_1/c$ (#14), $a$ = 10.696(2) Å, $b$ = 22.632(5) Å, $c$ = 11.846(3) Å, $\beta$ = 102.617(3)°, $V$ = 2798.4(10) Å$^3$, $\rho_{calcd}$ = 1.547 g/cm$^3$, $Z$ = 4, 22752 reflections measured, $R1$ = 0.0344 [$I > 2\sigma(I)$], and $wR2$ = 0.0905 (all reflections), GOF = 1.026.